Science
AAAS

Observation of Correlated Particle-Hole Pairs and String Order in Low-Dimensional Mott Insulators

M. Endres, *et al.*

Science **334**, 200 (2011);
DOI: 10.1126/science.1209284

of sub-femtosecond pump-probe interrogation of strong-field phenomena opens exciting research prospects. Real-time insight into multiple ionization in multi- to single-cycle laser fields, or into strong-field–induced electron correlations in atoms, molecules, or solids (*48*, *49*), are but a few examples.

References and Notes

1. J. F. Whitaker *et al.*, *Microelectron. Eng.* **12**, 369 (1990).
2. L. Xu *et al.*, *Opt. Lett.* **21**, 2008 (1996).
3. T. Brabec, F. Krausz, *Rev. Mod. Phys.* **72**, 545 (2000).
4. J. Reichert *et al.*, *Opt. Commun.* **172**, 59 (1999).
5. D. J. Jones *et al.*, *Science* **288**, 635 (2000).
6. S. A. Diddams *et al.*, *Phys. Rev. Lett.* **84**, 5102 (2000).
7. A. Apolonski *et al.*, *Phys. Rev. Lett.* **85**, 740 (2000).
8. T. Udem, R. Holzwarth, T. W. Hänsch, *Nature* **416**, 233 (2002).
9. S. T. Cundiff, J. Ye, *Rev. Mod. Phys.* **75**, 325 (2003).
10. A. Baltuška *et al.*, *Nature* **421**, 611 (2003).
11. M. Hentschel *et al.*, *Nature* **414**, 509 (2001).
12. R. Kienberger *et al.*, *Nature* **427**, 817 (2004).
13. G. Sansone *et al.*, *Science* **314**, 443 (2006).
14. E. Goulielmakis *et al.*, *Science* **320**, 1614 (2008).
15. M. F. Kling *et al.*, *Science* **312**, 246 (2006).
16. G. Sansone *et al.*, *Nature* **465**, 763 (2010).
17. M. Schultze *et al.*, *Science* **328**, 1658 (2010).
18. J. Mauritsson *et al.*, *Phys. Rev. Lett.* **105**, 053001 2010).
19. E. Goulielmakis *et al.*, *Nature* **466**, 739 (2010).
20. S. Zherebtsov *et al.*, *Nat. Phys.*, published online 24 April 2011 (10.1038/nphys1983).
21. P. Eckle *et al.*, *Science* **322**, 1525 (2008).
22. S. E. Harris, A. V. Sokolov, *Phys. Rev. Lett.* **81**, 2894 (1998).
23. A. V. Sokolov, D. R. Walker, D. D. Yavuz, G. Y. Yin, S. E. Harris, *Phys. Rev. Lett.* **85**, 562 (2000).
24. J. Q. Liang, M. Katsuragawa, F. L. Kien, K. Hakuta, *Phys. Rev. Lett.* **85**, 2474 (2000).
25. A. V. Sokolov, D. R. Walker, D. D. Yavuz, G. Y. Yin, S. E. Harris, *Phys. Rev. Lett.* **87**, 033402 (2001).
26. T. Suzuki, M. Hirai, M. Katsuragawa, *Phys. Rev. Lett.* **101**, 243602 (2008).
27. Z.-M. Hsieh *et al.*, *Phys. Rev. Lett.* **102**, 213902 (2009).
28. H.-S. Chan *et al.*, *Science* **331**, 1165 (2011).
29. R. K. Shelton *et al.*, *Science* **293**, 1286 (2001).
30. M. Yamashita, K. Yamane, R. Morita, *IEEE J. Sel. Top. Quantum Electron.* **12**, 213 (2006).
31. S. Rausch, T. Binhammer, A. Harth, F. X. Kärtner, U. Morgner, *Opt. Express* **16**, 17410 (2008).
32. G. Krauss *et al.*, *Nat. Photonics* **4**, 33 (2010).
33. K. Okamura, T. Kobayashi, *Opt. Lett.* **36**, 226 (2011).
34. E. Goulielmakis *et al.*, *Science* **317**, 769 (2007).
35. E. Goulielmakis *et al.*, *Science* **305**, 1267 (2004).
36. This indicates that relative to the ground state configuration, a hole (or electron vacancy) is created in the nl_j^{-1} nl subshell, where j denotes the total angular momentum and m_j its projection on the z axis, the latter being aligned with the laser polarization.
37. B. R. Mollow, *Phys. Rev. A* **5**, 1522 (1972).
38. T. Unold, K. Mueller, C. Lienau, T. Elsaesser, A. D. Wieck, *Phys. Rev. Lett.* **92**, 157401 (2004).
39. C. H. B. Cruz, J. P. Gordon, P. C. Becker, R. L. Fork, C. V. Shank, *Int. J. Quant. Elec.* **24**, 261 (1988).
40. S. H. Autler, C. H. Townes, *Phys. Rev.* **100**, 703 (1955).
41. B. J. Sussman, *Am. J. Phys.* **79**, 477 (2011).
42. N. B. Delone, V. P. Krainov, *Phys. Uspekhi* **169**, 753 (1999).
43. L. Greenman *et al.*, *Phys. Rev. A* **82**, 023406 (2010).
44. S. Pabst, L. Greenman, P. J. Ho, D. A. Mazziotti, R. Santra, *Phys. Rev. Lett.* **106**, 053003 (2011).
45. F. Remacle, M. Nest, R. D. Levine, *Phys. Rev. Lett.* **99**, 183902 (2007).
46. M. Meckel *et al.*, *Science* **320**, 1478 (2008).
47. O. Smirnova *et al.*, *Nature* **460**, 972 (2009).
48. M. Gertsvolf, M. Spanner, D. M. Rayner, P. B. Corkum, *J. Phys. B* **43**, 131002 (2010).
49. M. Durach, A. Rusina, M. F. Kling, M. I. Stockman, *Phys. Rev. Lett.* **105**, 086803 (2010).

Acknowledgments: We acknowledge the development of dedicated attosecond soft x-ray optics by M. Hofstetter and U. Kleineberg (LMU, MPQ). This work was supported by the Max Planck Society, the European Research Council grant (Attoelectronics-258501), the Deutsche Forschungsgemeinschaft Cluster of Excellence: Munich Centre for Advanced Photonics (www.munich-photonics.de), the King Saud University–MPQ collaboration, and the European Research Training Network ATTOFEL.

Supporting Online Material

www.sciencemag.org/cgi/content/full/science.1210268/DC1
SOM Text
Figs. S1 to S10
References (*50*–*59*)

24 June 2011; accepted 30 August 2011
Published online 1 September 2011;
10.1126/science.1210268

REPORTS

Observation of Correlated Particle-Hole Pairs and String Order in Low-Dimensional Mott Insulators

M. Endres,[1]* M. Cheneau,[1] T. Fukuhara,[1] C. Weitenberg,[1] P. Schauß,[1] C. Gross,[1] L. Mazza,[1] M. C. Bañuls,[1] L. Pollet,[2] I. Bloch,[1,3] S. Kuhr[1,4]

Quantum phases of matter are characterized by the underlying correlations of the many-body system. Although this is typically captured by a local order parameter, it has been shown that a broad class of many-body systems possesses a hidden nonlocal order. In the case of bosonic Mott insulators, the ground state properties are governed by quantum fluctuations in the form of correlated particle-hole pairs that lead to the emergence of a nonlocal string order in one dimension. By using high-resolution imaging of low-dimensional quantum gases in an optical lattice, we directly detect these pairs with single-site and single-particle sensitivity and observe string order in the one-dimensional case.

The realization of strongly correlated quantum many-body systems using ultracold atoms has enabled the direct observation and control of fundamental quantum effects (*1*–*3*). A prominent example is the transition from a superfluid (SF) to a Mott insulator (MI), occurring when interactions between bosonic particles on a lattice dominate over their kinetic energy (*4*–*8*). At zero temperature and in the limit where the ratio of kinetic energy over interaction energy vanishes, particle fluctuations are completely suppressed and the lattice sites are occupied by an integer number of particles. However, at a finite tunnel coupling but still in the Mott insulating regime, quantum fluctuations create correlated particle-hole pairs on top of this fixed-density background, which can be understood as virtual excitations. These particle-hole pairs fundamentally determine the properties of the MI, such as its residual phase coherence (*9*), and lie at the heart of superexchange-mediated spin interactions that form the basis of quantum magnetism in multicomponent quantum gas mixtures (*10*–*12*).

In a one-dimensional system, the appearance of correlated particle-hole pairs at the transition point from a SF to a MI is intimately connected to the emergence of a hidden string-order parameter $\mathcal{O}_{\mathrm{P}}$ (*13*, *14*):

$$\mathcal{O}_{\mathrm{P}}^2 = \lim_{l\to\infty} \mathcal{O}_{\mathrm{P}}^2(l) = \lim_{l\to\infty} \left\langle \prod_{k\le j\le k+l} e^{i\pi\delta\hat{n}_j} \right\rangle \quad (1)$$

Here, $\delta\hat{n}_j = \hat{n}_j - \overline{n}$ denotes the deviation in occupation of the jth lattice site from the average background density, and k is an arbitrary position along the chain. In the simplest case of a MI with unity filling ($\overline{n} = 1$), relevant to our experiments, each factor in the product of operators in Eq. 1 yields −1 instead of +1 when a single-particle fluctuation from the unit back-

[1]Max-Planck-Institut für Quantenoptik, 85748 Garching, Germany. [2]Theoretische Physik, Eidgenössische Technische Hochschule (ETH) Zurich, 8093 Zurich, Switzerland. [3]Ludwig-Maximilians-Universität, 80799 Munich, Germany. [4]University of Strathclyde, Scottish Universities Physics Alliance, Glasgow G4 0NG, UK.

*To whom correspondence should be addressed. E-mail: manuel.endres@mpq.mpg.de

ground density is encountered. In the SF, particle and hole fluctuations occur independently and are uncorrelated, such that $\mathcal{O}_P = 0$. However, in the Mott insulating phase, density fluctuations always occur as correlated particle-hole pairs, resulting in $\mathcal{O}_P \neq 0$. For a homogeneous system, $\mathcal{O}_P$ is expected to follow a scaling of Berezinskii-Kosterlitz-Thouless (BKT) type (*15*). Nonlocal correlation functions, like the string-order parameter defined above, have been introduced in the context of low-dimensional quantum systems. They classify many-body quantum phases that are not amenable to a description through a local order parameter, typically used in the Landau paradigm of phase transitions. Examples include spin-1 chains (*16*) and spin-1/2 ladders (*17*), fermionic Mott and band insulators (*18*), and Haldane insulators in one-dimensional Bose gases (*13*, *14*). Recently, the intimate connection of string order and local symmetries has been uncovered (*19*), and wide-ranging classification schemes for quantum phases using such symmetry principles have been introduced (*20*, *21*). We show that correlated particle-hole pairs and string order can be directly detected by using single-atom–resolved images of strongly correlated ultracold quantum gases (*22*, *23*).

We prepared a two-dimensional degenerate gas of ultracold ^{87}Rb atoms before shining in a two-dimensional square optical lattice (lattice spacing a_{lat} = 532 nm) with variable lattice depths in x and y directions (*23*, *24*). A microscope objective with a resolution comparable to the lattice spacing was used for fluorescence detection of individual atoms. Because inelastic light-assisted collisions during the imaging lead to a rapid loss of atom pairs, our scheme detects the parity of the atom number. We used an algorithm to deconvolve the images, yielding single-site–resolved information of the on-site parity. Typically, our samples contained 150 to 200 atoms in order to avoid MIs of occupation numbers $\overline{n} > 1$.

To detect particle-hole pairs, we evaluated two-site parity correlation functions (*25*)

$$C(d) = \langle \hat{s}_k \hat{s}_{k+d} \rangle - \langle \hat{s}_k \rangle \langle \hat{s}_{k+d} \rangle \qquad (2)$$

where $\hat{s}_k = e^{i\pi\delta\hat{n}_k}$ is the parity operator at site k and d is the distance between the lattice sites. For the case of $\overline{n} = 1$, $\hat{s}_k$ yields +1 for an odd occupation number n_k and −1 for an even n_k. If a particle-hole pair exists on sites k and $k + d$, the same parity $s(n_k) = s(n_{k+d}) = -1$ is detected (Fig. 1). The existence of correlated particle-hole pairs therefore leads to an increase of $\langle \hat{s}_k \hat{s}_{k+d} \rangle$ above the factorized form $\langle \hat{s}_k \rangle \langle \hat{s}_{k+d} \rangle$, which results from uncorrelated fluctuations, for example, because of thermal excitations. We obtained $C(d)$ from our deconvolved images by an average over many experimental realizations and by an additional average over k in a central region of interest.

We first analyzed two-site parity correlations in one-dimensional systems (Fig. 2, A and B). To create isolated one-dimensional tubes, we kept the lattice axis along y at a constant depth of V_y = 17(1) E_r, where $E_r = h^2/(8ma_{lat}^2)$ denotes the recoil energy and m is the atomic mass of ^{87}Rb. Experimental uncertainties are marked as terms in parentheses following numerical values. We recorded the nearest-neighbor correlations $C(d = 1)$ for different values of J/U along the direction of the one-dimensional tubes (red circles in Fig. 2B), where J and U are the tunneling matrix element and the on-site interaction energy in the Bose-Hubbard model, respectively (*24*). For small J/U, the nearest-neighbor correlations vanish, because only uncorrelated thermal excitations exist deep in the MI regime. Because particle-hole pairs emerge with increasing J/U, we observe an increase of nearest-neighbor correlations until a peak value is reached, well before the critical value $(J/U)_c^{1d} \approx 0.3$ (*26*, *27*) for the one-dimensional SF-MI transition. The observed signal is a genuine quantum effect because thermally induced particle-hole pairs extend over arbitrary distances and are therefore uncorrelated. Their presence leads to a reduction of the correlation signal. We found no correlations when performing the same analysis perpendicular to the one-dimensional tubes (blue circles in Fig. 2B), showing that the coupling between the tubes was negligible.

Our data show very good agreement with ab initio finite-temperature matrix product state (MPS) calculations (*28*, *29*) at temperature T = 0.09 U/k_B (where k_B is Boltzman's constant) (Fig. 2A, solid line) that also take into account our harmonic trapping potential with frequency $\omega/(2\pi)$ = 60(1) Hz. Compared with a homogeneous system at T = 0 (dashed line), the experimental signal is reduced, especially around the maximum. This reduction can be attributed in equal parts to the finite temperature of our system and the averaging over different local chemical potentials. The latter is especially severe in the one-dimensional case owing to the narrow width of the Mott lobe for $\overline{n} = 1$ close to the critical point (*15*). Interestingly, the growth of particle-hole correlations $\propto J^2/U^2$ expected from first-order perturbation theory (*24*) is limited to very small values, $J/U < 0.05$, before deviations in the experiment and the numerical simulations are observed.

Because the dimensionality of the system plays an important role in its correlation properties, we also measured the two-site parity correlations across the two-dimensional SF-MI transition by simultaneously varying J/U along both lattice axes (Fig. 2C). In contrast to the one-dimensional case, we now observe the same nearest-neighbor correlations within our error bars along both axes. The maximum correlations are smaller than in one dimension, and the peak value is now reached around the critical value $(J/U)_c^{2d} \approx 0.06$ (*30*). We compared our data with quantum Monte Carlo (QMC) simulations for a homogeneous system at T = 0.1 U/k_B (solid line in Fig. 2C) and found good quantitative agreement. Here, the broader shape of the Mott lobe leads to a weaker

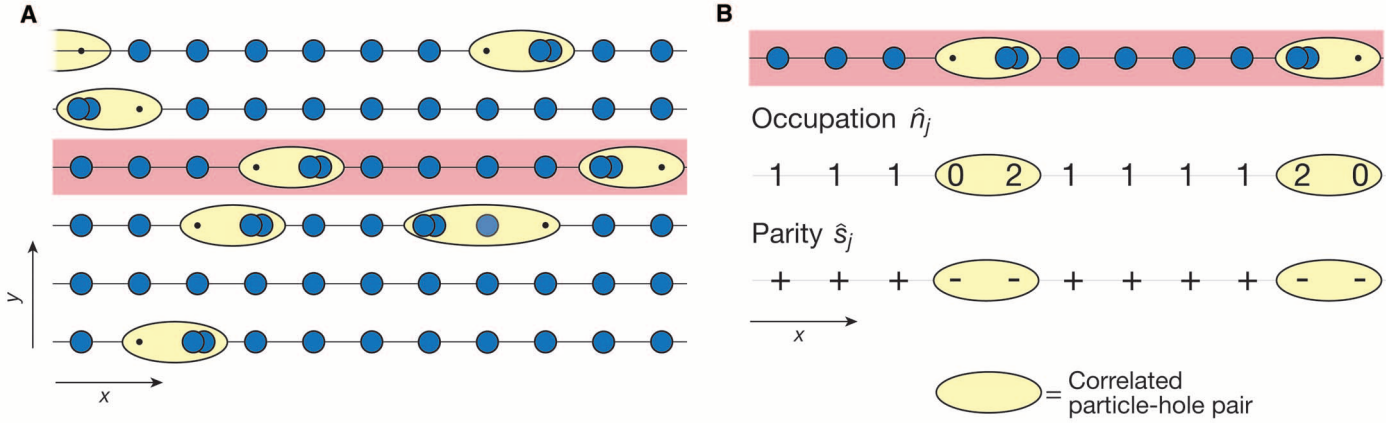

Fig. 1. Quantum-correlated particle-hole pairs in one-dimensional MIs. (**A**) In a two-dimensional array of atoms (blue circles), decoupled one-dimensional systems were created by suppressing tunneling along the y direction. Quantum fluctuations then only induce correlated particle-hole excitations (yellow ellipses) along the x direction of the one-dimensional MIs. (**B**) Such correlated fluctuations in the occupation $\hat{n}_j$ are detected in the experiment as correlated fluctuations in the parity $\hat{s}_j$. The light red bar in (A) marks the one-dimensional chain chosen in (B) for further explanations.

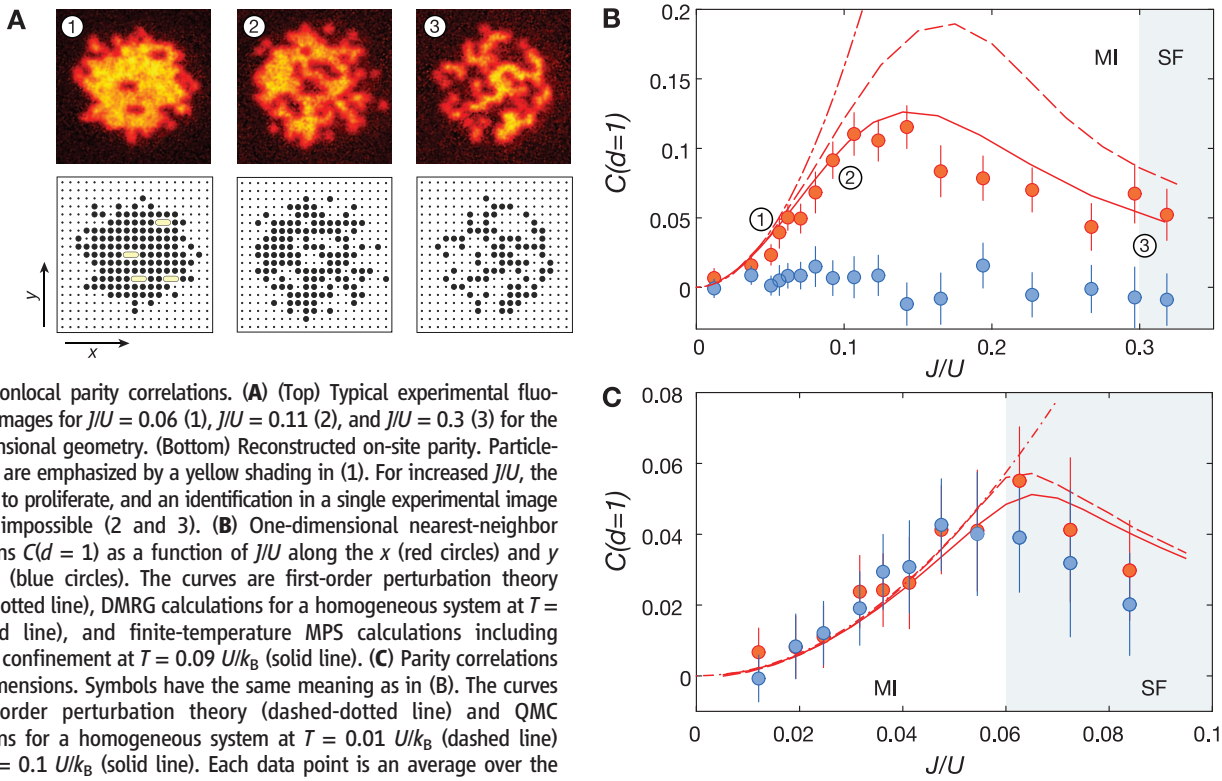

Fig. 2. Nonlocal parity correlations. **(A)** (Top) Typical experimental fluorescence images for $J/U = 0.06$ (1), $J/U = 0.11$ (2), and $J/U = 0.3$ (3) for the one-dimensional geometry. (Bottom) Reconstructed on-site parity. Particle-hole pairs are emphasized by a yellow shading in (1). For increased J/U, the pairs start to proliferate, and an identification in a single experimental image becomes impossible (2 and 3). **(B)** One-dimensional nearest-neighbor correlations $C(d = 1)$ as a function of J/U along the x (red circles) and y directions (blue circles). The curves are first-order perturbation theory (dashed-dotted line), DMRG calculations for a homogeneous system at $T = 0$ (dashed line), and finite-temperature MPS calculations including harmonic confinement at $T = 0.09\ U/k_B$ (solid line). **(C)** Parity correlations in two dimensions. Symbols have the same meaning as in (B). The curves are first-order perturbation theory (dashed-dotted line) and QMC calculations for a homogeneous system at $T = 0.01\ U/k_B$ (dashed line) and at $T = 0.1\ U/k_B$ (solid line). Each data point is an average over the central nine-by-seven lattice sites from 50 to 100 pictures. The error bars denote the 1σ statistical uncertainty. The light blue shading highlights the SF phase.

averaging effect over different local chemical potentials. The increased strength of the correlations and the larger shift of the maximum of the correlations relative to the critical point in the one-dimensional case directly reflect the more prominent role of quantum fluctuations in lower dimensions. This can also be seen from the on-site fluctuations $C(d = 0)$ at the critical point, which are increased in the one-dimensional case (*24*). In both the one-dimensional and the two-dimensional systems, two-site correlations are expected to decay strongly with distance. Our data for the next-nearest-neighbor correlations $C(d = 2)$ are consistent with this predicted behavior (*24*).

In addition to two-site correlations, we evaluated string-type correlators $\mathcal{O}_P^2(l) = \langle \prod_{j=k}^{k+l} \hat{s}_j \rangle$ (Eq. 1 and Fig. 1B) in our one-dimensional systems, where the product is calculated over a chain of length $l + 1$. In the simplest case of a zero-temperature MI at $J/U = 0$, no fluctuations exist and therefore $\mathcal{O}_P^2(l) = 1$. As J/U increases, fluctuations in the form of particle-hole pairs appear. Whenever a certain number of particle-hole pairs lies completely within the region covered by the string correlator, the respective minus signs cancel pairwise. However, there is also the possibility that a particle-hole pair is cut by one end of the string correlator, for example, when a particle exists at position $< k$ and the corresponding hole has a position $\geq k$, resulting in an unpaired minus sign. As a consequence, $\mathcal{O}_P^2(l)$ decreases with increasing J/U because the probability to cut particle-hole pairs becomes larger. Finally, at the transition to the SF phase, the pairs begin to deconfine and overlap, resulting in a completely random product of signs and $\mathcal{O}_P^2 = 0$.

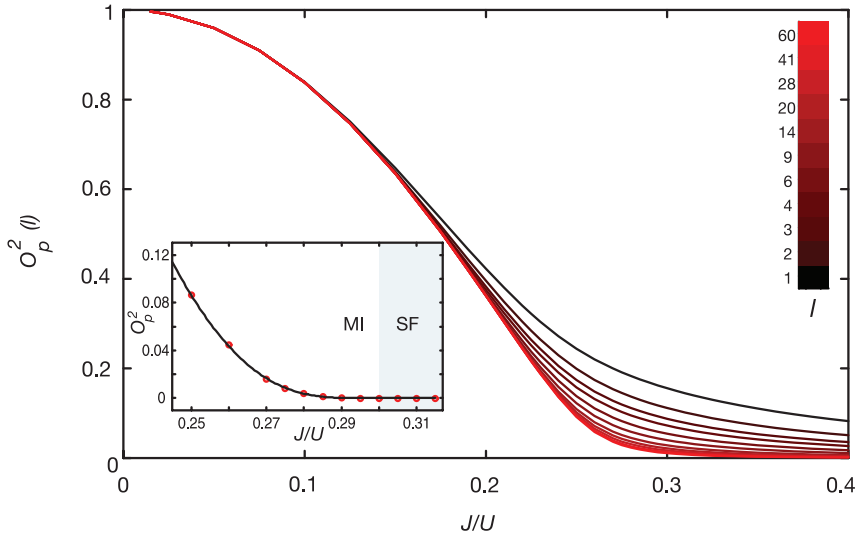

Fig. 3. Numerical calculation of the string-order parameter. $\mathcal{O}_P^2(l)$ is shown as a function of J/U calculated with DMRG for a homogeneous chain ($\bar{n} = 1$, $T = 0$) of total length 216. Lines show $\mathcal{O}_P^2(l)$ for selected l (black to red colors). **(Inset)** Extrapolated values of $\mathcal{O}_P^2 = \lim_{l\to\infty} \mathcal{O}_P^2(l)$ together with a fit (black line) of the form $\mathcal{O}_P^2 \propto \exp\left\{-A\left[(J/U)_c^{1d} - (J/U)\right]^{-1/2}\right\}$, characteristic for a transition of BKT type (*24*).

To support this intuitive argument, we calculated $\mathcal{O}_P^2(l)$ numerically by using density-matrix renormalization group (DMRG) in a homogeneous system at $T = 0$. We show $\mathcal{O}_P^2(l)$ in Fig. 3 for selected distances of l together with the extrapolated values of $\mathcal{O}_P^2 = \lim_{l\to\infty} \mathcal{O}_P^2(l)$ (Fig. 3 inset), which we computed by using finite-size scaling (*24*). We performed a fit to the extrapolated values close to the critical point with an exponential scaling $\mathcal{O}_P^2 \propto \exp\left\{-A[(J/U)_c^{1d} - (J/U)]^{-1/2}\right\}$ characteristic for a transition of BKT type (Fig. 3)

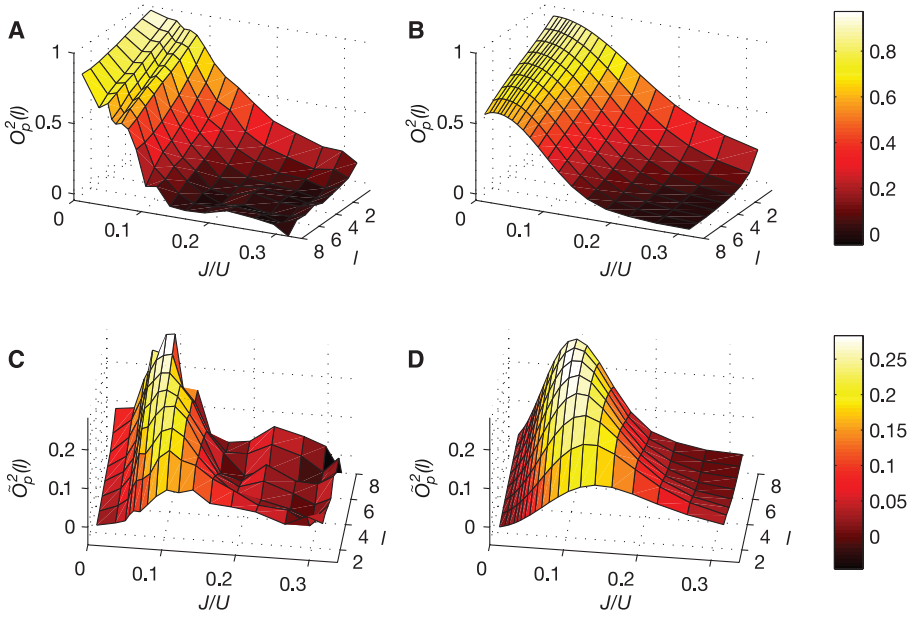

Fig. 4. String correlators. (**A**) Experimental values of $\mathcal{O}_P^2(l)$ for $0 \le l \le 8$. (**B**) In-trap MPS calculations at $T = 0.09\ U/k_B$. (**C**) Experimentally determined string correlator $\tilde{\mathcal{O}}_P^2(l)$ as defined in Eq. 3 for lengths $1 \le l \le 8$ (**D**) In-trap MPS calculations at $T = 0.09\ U/k_B$. The l axes in (C) and (D) have been inverted.

that one expects in one dimension (*14*, *15*). From the fit, we find $(J/U)_c^{1d} = 0.295 - 0.320$, which is compatible with previously computed values (*26*, *27*, *24*). The fact that $\mathcal{O}_P = 0$ in the SF and $\mathcal{O}_P > 0$ in the MI as well as the agreement with the expected scaling show that $\mathcal{O}_P$ serves as an order parameter for the MI phase in one dimension (*14*). Additionally, the simulations demonstrate that $\mathcal{O}_P(l)$ is well suited to characterize the SF-MI transition even for finite l.

Our experimentally obtained values of $\mathcal{O}_P^2(l)$ for string length $l \le 8$ (Fig. 4A) agree qualitatively well with in-trap MPS calculations at $T = 0.09\ U/k_B$ (Fig. 4B). We observe a stronger decay of $\mathcal{O}_P^2(l)$ with l compared to the $T = 0$ case, because at finite temperature thermal fluctuations lead to minus signs at random positions of the chain and reduce the average value of $\mathcal{O}_P^2(l)$. Despite that, we still see a strong growth of $\mathcal{O}_P^2(l)$, once the transition from the SF to the MI is crossed, with a similar behavior as in Fig. 3.

For a completely uncorrelated state, $\mathcal{O}_P^2(l)$ factorizes to $\prod_{k \le j \le k+l} \langle \hat{s}_j \rangle$, and in a homogeneous system we would expect a decay with string length of the form $\langle \hat{s}_j \rangle^{l+1}$, which can be slow provided the mean on-site parity $\langle \hat{s}_j \rangle$ is close to one. To rule out that our experimental data shows only such a trivial behavior, we define a new quantity $\tilde{\mathcal{O}}_P^2(l)$ that more naturally reflects the underlying correlations:

$$\tilde{\mathcal{O}}_P^2(l) = \mathcal{O}_P^2(l) - \prod_{k \le j \le k+l} \langle \hat{s}_j \rangle \qquad (3)$$

First, we notice that $\tilde{\mathcal{O}}_P^2(l)$ for $l = 1$ is equal to the two-site correlation function $C(d = 1)$. Second, $\tilde{\mathcal{O}}_P^2(l) \approx \mathcal{O}_P^2(l)$ for long distances l because $\prod_{k \le j \le k+l} \langle \hat{s}_j \rangle$ eventually decays to zero (except for the singular case $J/U = 0$ and $T = 0$). The correlation function $\tilde{\mathcal{O}}_P^2(l)$ can therefore be understood as an extension of the two-site correlation function that essentially captures the physics behind string order in one-dimensional MIs.

Experimental and theoretical values for $\tilde{\mathcal{O}}_P^2(l)$ are shown in Fig. 4, C and D. For small J/U, $\tilde{\mathcal{O}}_P^2(l)$ is reduced compared with $\mathcal{O}_P^2(l)$ because few particle-hole pairs exist and $\mathcal{O}_P^2(l)$ is close to its factorized form for short values of l. In the case of vanishing J/U, we even expect $\tilde{\mathcal{O}}_P^2(l) = 0$ because all sites are completely decoupled. For intermediate $J/U \approx 0.1$, $\tilde{\mathcal{O}}_P^2(l)$ grows rapidly with l showing a strong deviation from the factorized form. Lastly, in the SF regime, $\tilde{\mathcal{O}}_P^2(l)$ becomes indiscernible from zero for large lengths in contrast to the nearest-neighbor two-site correlation function. Furthermore, our data show a genuine three-site correlation, which we revealed after subtracting all two-site correlators in addition to local terms (*24*).

We have shown direct measurements of nonlocal parity-parity correlation functions on the single–lattice-site and single-atom level, and we demonstrated that a one-dimensional MI is characterized by nonlocal string order. A natural extension of our work would be to reveal, for example, topological quantum phases such as the Haldane insulator of bosonic atoms (*13*, *14*). A Haldane insulator exhibits a hidden antiferromagnetic ordering and is expected to occur in one-dimensional quantum gases in the presence of longer ranged interactions, which could be realized in our experiment by using Rydberg atoms (*31*).

References and Notes

1. D. Jaksch, P. Zoller, *Ann. Phys.* **315**, 52 (2005).
2. M. Lewenstein *et al.*, *Adv. Phys.* **56**, 243 (2007).
3. I. Bloch, J. Dalibard, W. Zwerger, *Rev. Mod. Phys.* **80**, 885 (2008).
4. M. P. A. Fisher, P. B. Weichman, G. Grinstein, D. S. Fisher, *Phys. Rev. B* **40**, 546 (1989).
5. D. Jaksch, C. Bruder, J. I. Cirac, C. Gardiner, P. Zoller, *Phys. Rev. Lett.* **81**, 3108 (1998).
6. M. Greiner, O. Mandel, T. Esslinger, T. W. Hänsch, I. Bloch, *Nature* **415**, 39 (2002).
7. T. Stöferle, H. Moritz, C. Schori, M. Köhl, T. Esslinger, *Phys. Rev. Lett.* **92**, 130403 (2004).
8. I. B. Spielman, W. D. Phillips, J. V. Porto, *Phys. Rev. Lett.* **98**, 080404 (2007).
9. F. Gerbier *et al.*, *Phys. Rev. Lett.* **95**, 050404 (2005).
10. A. B. Kuklov, B. V. Svistunov, *Phys. Rev. Lett.* **90**, 100401 (2003).
11. L.-M. Duan, E. Demler, M. D. Lukin, *Phys. Rev. Lett.* **91**, 090402 (2003).
12. S. Trotzky *et al.*, *Science* **319**, 295 (2008); 10.1126/science.1150841.
13. E. G. Dalla Torre, E. Berg, E. Altman, *Phys. Rev. Lett.* **97**, 260401 (2006).
14. E. Berg, E. Dalla Torre, T. Giamarchi, E. Altman, *Phys. Rev. B* **77**, 245119 (2008).
15. T. Kühner, H. Monien, *Phys. Rev. B* **58**, R14741 (1998).
16. M. den Nijs, K. Rommelse, *Phys. Rev. B* **40**, 4709 (1989).
17. E. Kim, G. Fáth, J. Sólyom, D. Scalapino, *Phys. Rev. B* **62**, 14965 (2000).
18. F. Anfuso, A. Rosch, *Phys. Rev. B* **75**, 144420 (2007).
19. D. Pérez-García, M. M. Wolf, M. Sanz, F. Verstraete, J. I. Cirac, *Phys. Rev. Lett.* **100**, 167202 (2008).
20. X. Chen, Z.-C. Gu, X.-G. Wen, *Phys. Rev. B* **83**, 035107 (2011).
21. N. Schuch, D. Pérez-García, J. I. Cirac, (2010); http://arxiv.org/abs/1010.3732.
22. W. S. Bakr *et al.*, *Science* **329**, 547 (2010); 10.1126/science.1192368.
23. J. F. Sherson *et al.*, *Nature* **467**, 68 (2010).
24. Materials and methods are available as supporting material on *Science* Online.
25. E. Kapit, E. Mueller, *Phys. Rev. A* **82**, 013644 (2010).
26. T. D. Kühner, S. R. White, H. Monien, *Phys. Rev. B* **61**, 12474 (2000).
27. V. Kashurnikov, A. Krasavin, B. Svistunov, *JETP Lett.* **64**, 99 (1996).
28. F. Verstraete, J. J. García-Ripoll, J. I. Cirac, *Phys. Rev. Lett.* **93**, 207204 (2004).
29. M. Zwolak, G. Vidal, *Phys. Rev. Lett.* **93**, 207205 (2004).
30. B. Capogrosso-Sansone, S. Söyler, N. Prokof'ev, B. Svistunov, *Phys. Rev. A* **77**, 015602 (2008).
31. M. Saffman, T. Walker, K. Mølmer, *Rev. Mod. Phys.* **82**, 2313 (2010).

Acknowledgments: We acknowledge helpful discussions with E. Altman, E. Dalla Torre, M. Rizzi, and I. Cirac. This work was supported by Max-Planck-Gesellschaft, Deutsche Forschungsgemeinschaft, European Union (NAMEQUAM, AQUTE, and Marie Curie Fellowship to M.C.), and Japan Society for Promotion of Science (Postdoctoral Fellowship for Research Abroad to T.F.). L.P. is supported by the Swiss National Science Foundation under grant PZ00P2-131892/1. DMRG simulations were performed with use of code released within the PwP project (www.qti.sns.it). QMC calculations were performed on the Brutus cluster at ETH Zurich.

Supporting Online Material

www.sciencemag.org/cgi/content/full/334/6053/200/DC1
Materials and Methods
SOM Text
Figs. S1 to S3
Table S1
References (*32*–*42*)

2 June 2011; accepted 15 August 2011
10.1126/science.1209284